Article

pubs.acs.org/Biomac

Controlling Self-Assembling Peptide Hydrogel Properties through Network Topology

Jie Gao,[†,‡,§] Claire Tang,[†,‡] Mohamed Elsawy,[†,‡] Andrew M. Smith,[†,‡] Aline F. Miller,[‡,∥] and Alberto Saiani*[,†,‡]

[†]School of Materials, [‡]Manchester Institute of Biotechnology, and [∥]School of Chemical Engineering and Analytical Sciences, The University of Manchester, Oxford Road, Manchester, M13 9PL, United Kingdom

Supporting Information

ABSTRACT: Self-assembling peptide-based hydrogels have encountered increasing interest in the recent years as scaffolds for 3D cell culture or for controlled drug delivery. One of the main challenges is the fine control of the mechanical properties of these materials. The bulk properties of hydrogels not only depend on the intrinsic properties of the fibers but also on the network topology formed. In this work we show how fiber−fiber interactions can be manipulated by design to control the final hydrogel network topology and therefore control the final properties of the material. This was achieved by exploiting the design features of β-sheet forming peptides based on hydrophobic and hydrophilic residue alternation and exploiting the ability of the arginine's guanidine side group to interact with itself and with other amino acid side groups. By designing octa-peptides based on phenylalanine, glutamic acid, lysine, and arginine, we have investigated how fiber association and bundling affect the dynamic shear modulus of hydrogels and how it can be controlled by design. This work opens the possibility to fine-tune by design the bulk properties of peptide hydrogels.

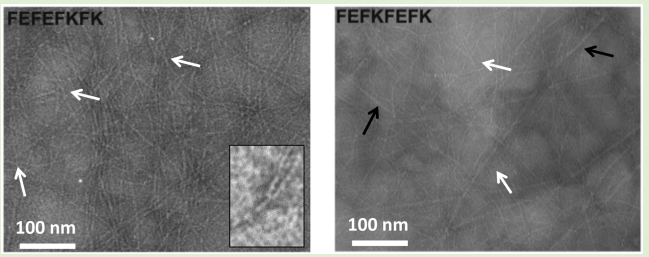

INTRODUCTION

The use of noncovalent self-assembly to construct materials has become a prominent strategy in material science offering practical routes for the construction of increasingly functional materials for a variety of applications ranging from electronics to biotechnology.[1−4] A variety of molecular building blocks can be used for this purpose; one such block that has attracted considerable attention in the last 20 years is de novo designed self-assembling peptides.[5−8] One particular class of materials with significant potential in the biological and biomedical fields are self-assembling peptide based hydrogels. These highly hydrated, biodegradable and biocompatible "soft" materials are very attractive for the design of scaffolds for the 3D culture of cells[9−11] and delivery of drugs.[12,13] A number of self-assembling peptide designs have emerged in the literature that allow the fabrication of very stable hydrogels. One of the main challenges that remain in the field is the fine-tuning of the mechanical properties of these hydrogels as different cell types, and therapeutic approaches require hydrogels with different properties.

The formation of hydrogels by self-assembling peptides involves two distinct processes; the self-assembly of the peptides themselves to form thin fibrillar structures and the entanglement and association of these fibrils into a three-dimensional percolated network (Figure 1). Developing a fundamental understanding of these two processes at all length scales is crucial as the properties of the final materials will not only depend on the intrinsic properties of the fibers, but also on how they assemble and ultimately on the properties of the network formed. Most of the focus in the literature is on the first process, the self-assembly of the peptides into fibers. The second process has been less studied and is less well understood and is the focus of this work.

We have investigated in recent years the self-assembly of a family of amphipathic short β-sheet forming peptides inspired from Zhang's group work.[14−20] These peptides are typically 8−16 residues long and their design is based on the alternation of hydrophobic and hydrophilic amino acids. These peptides are well-known to readily self-assemble into antiparallel β-sheets and form, above a critical gelation concentration (CGC), hydrogels that have been shown to support the growth of a variety of cells,[21−27] as well as allow the controlled delivery of a variety of drugs.[12,28−31] One interesting aspect of this design is that formation of these sheets results in all the hydrophobic side groups being located on the same face of the sheet, while all the hydrophilic side groups are located on the opposite face.[32−35] As a result it is speculated that two of these sheets associate through their hydrophobic faces to form a fiber. Above the CGC these fibers entangle and/or associate to form a 3D percolated network that traps water, that is, a hydrogel (Figure 1). As a consequence interfiber interactions which play

Received: November 15, 2016
Revised: January 6, 2017
Published: January 9, 2017

DOI: 10.1021/acs.biomac.6b01693
Biomacromolecules XXXX, XXX, XXX−XXX

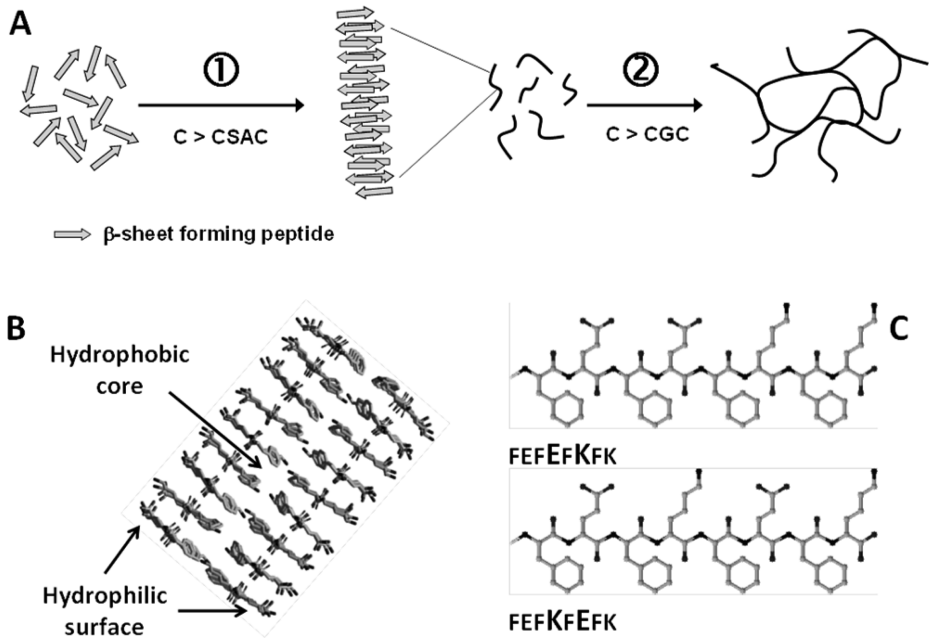

Figure 1. (A) Schematic representation of the self-assembly and gelation process of β-sheet forming peptides. (B) Schematic representation of β-sheet fibers. (C) Chemical structure of lysine containing peptides.

a key role in the fibrillar network formation are mainly controlled by the hydrophilic residues.

In this work we were interested in understanding how network topology affects the mechanical properties of the hydrogel and how it can be used to design materials with tailored properties. For this purpose we decided to use a family of octapeptides based on the same design that are known to self-assemble into β-sheet rich fibrils. This approach allowed us to keep the fiber structure identical across all the systems and focus on the effect of network topology on the mechanical properties of the hydrogels formed. As mentioned above due to the design chosen interfiber interactions are controlled mainly by the hydrophilic residues. Of particular interest to us was arginine, which is a residue that has a guanidine side group. This side group can interact strongly with other amino acid side groups as well as with itself in a variety of configurations, including through hydrogen bonding and electrostatic interactions, as well as salt bridges.[36−38] Our hypothesis was that the introduction of this amino acid would result in increased fiber−fiber interactions and therefore would affect the topology of the network formed and the final mechanical properties of the hydrogels. For this purpose a family of phenylalanine based peptides containing lysine (K) and arginine (R) were designed. Hydrogels were prepared and characterized using a range of techniques including Fourier transform infrared spectroscopy (FTIR), small angle neutron scattering (SANS), transmission electron microscopy (TEM), and oscillatory shear rheology.

MATERIALS AND METHODS

Materials. Peptides were purchased as TFA salts from Cambridge Research Biochemicals (U.K.; FEFEFKFK and FEFKFEFK) and Biomatik (U.S.A.; FEFEFRFK and FEFEFRFR) and used without further purification. The purity of the compounds was verified by HPLC (>95%; see Supporting Information (SI) for HPLC traces) and mass spectrometry. HPLC grade and deuterated (99.9 atom % D) water were purchased from Sigma-Aldrich (U.K.).

Sample Preparation. Depending on the desired formulation and concentration the required amount of peptide(s) powders (or powder mixtures) was suspended in HPLC grade water. The samples were vortexed and sonicated (VWR ultrasonicator bath, 30 W) until the peptide(s) was fully dissolved. Due to presence of TFA (typically 3:1 TFA to peptide ratio as the TFA is bound to the two cationic residues as well as the terminal NH_3^+ end group), the pH of the sample was 2.3−2.8. In order to have a common pH for all the samples, their pH was adjusted to 3.0 using a 1 M solution of NaOH (typically ∼10−20 μL added, depending on starting pH). The samples were then stored at room temperature overnight, and the pH was checked again before use.

Phase Diagram. The samples were prepared in a test tube as described above and placed in a water bath, the temperature of which was controlled by both mercury and Grant analogue thermometers. The temperature of the bath was increased from 25 to 90 °C by steps of 5 °C. The samples were left to equilibrate at each temperature for 15 min before their macroscopic state was assessed through the "test-tube tilting" method.

Fourier Transform Infrared Spectroscopy (FTIR). Multiple bounce attenuated total reflectance (ATR) FTIR experiments were undertaken using samples prepared in water. Spectra were recorded on a Thermo Nicolet 5700 spectrometer equipped with a trough plate comprising of a zinc selenide crystal, which permitted 12 reflections with a 45° angle of incidence. The samples were spread directly on the surface of the trough plate. Spectra were acquired in the 4000−400 cm^{-1} range with a resolution of 4 cm^{-1} over 256 scans. The water spectrum was used as background and subtracted from all spectra using Omnic software (version 7.2, Thermo Electron Corporation) provided with the instrument.

Dynamic Oscillatory Shear Rheometry. Viscoelastic properties were assessed in an oscillatory mode, using a stress-controlled rheometer (TA Instruments AR-G2) equipped with a Peltier plate to control temperature. A parallel plate geometry was used with a diameter of 20 mm and a gap of 250 μm. To ensure the measurements were made in the linear regime, amplitude sweeps were performed and showed no variation in G' and G'' up to a strain of 1%. The dynamic shear moduli of the hydrogel were measured at 1 Hz with a strain of 0.1%. All experiments were performed at 25 °C at least three times to ensure reproducibility.

Transmission Electron Microscopy (TEM). Samples were prepared at 10 mg mL^{-1} and diluted 10-fold. The solutions were vortexed until they were fully homogeneous. A total of 20 μL of sample was adsorbed onto the glow-discharged, carbon-coated copper

DOI: 10.1021/acs.biomac.6b01693
Biomacromolecules XXXX, XXX, XXX−XXX

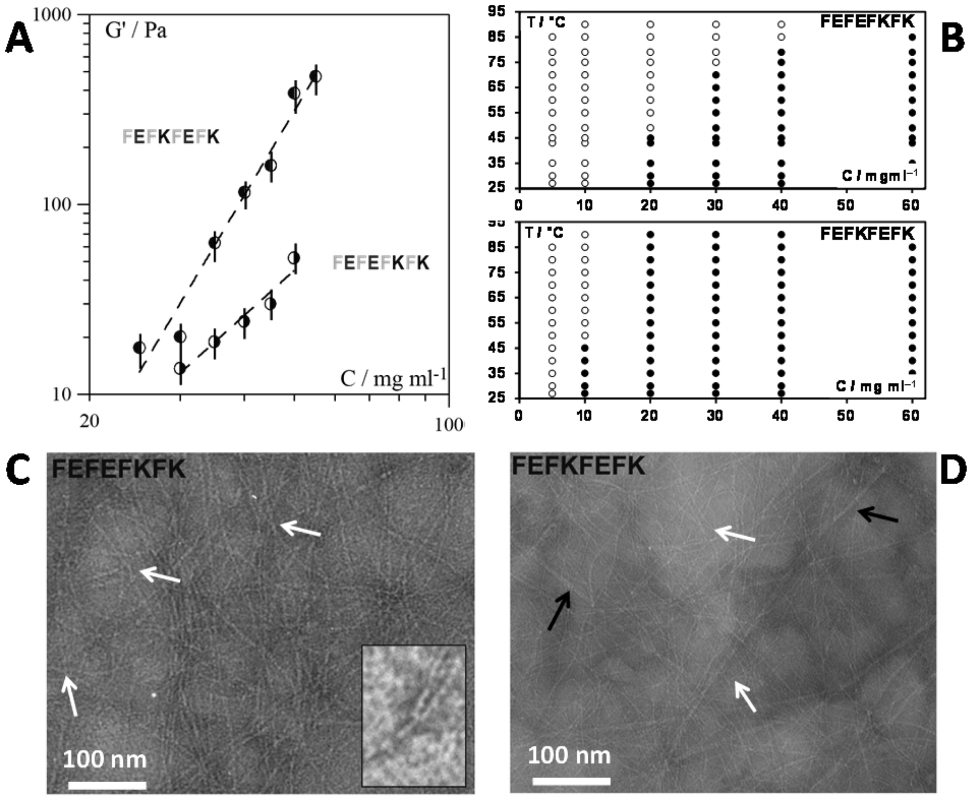

Figure 2. (A) Dynamic shear moduli of lysine based peptide hydrogels (see Figure 1 for chemical structures). (B) Temperature vs concentration phase diagrams (open symbols: liquid/viscous liquid and closed symbols weak gels/gels). (C, D) TEM images obtained for FEF**E**F**K**FK (C: inset, high resolution image showing details of a "Y" junction) and FEF**K**F**E**FK samples (D). White arrows show "Y" junction point, while black arrows show associated fibers. For more information, see text.

grid (400 mesh, Agar Scientific) for 30 s. The loaded grids were washed in distilled water for 15 s and negatively stained with 20 μL of 1% (w/v) uranyl acetate. The grids were then blotted on Whatman 50 filter paper and allowed to air-dry for 30 min prior to observation. Data was collected at high vacuum on a FEI Tecnai12 BioTwin transmission electron microscope connected to a high resolution Orius CCD SC1000 camera.

Small Angle Neutron Scattering (SANS). SANS experiments were performed at the Forshungszentrum Jülich (FRJ-2) on diffractometer KWS-2. The white beam was monochromated with a velocity selector by Dornier. The neutron wavelength was $\lambda = 0.48$ nm with a wavelength distribution characterized by a full width at half-maximum $\Delta\lambda/\lambda = 0.1$. Samples were irradiated on an area of 0.8 × 0.8 cm^2. The beamline was equipped with a two-dimensional detector with a 50 × 50 cm^2 active area with a spatial resolution of 0.8 × 0.8 cm^2 (further details are available on request at Forshungszentrum Jülich). By varying the sample−detector distance, the available momentum transfer vector (q) was in the range of $0.1 < q$ (nm^{-1}) < 2.4, with $q = (4\pi/\lambda)\sin(\theta/2)$, where θ is the scattering angle. The collected data was corrected for the detector efficiency and dark current background. Counter normalization was achieved by using the incoherent scattering of an amorphous hydrogenous poly(methyl methacrylate) secondary standard. After ensuring the scattering was isotropic, the data were radially averaged to obtain a one-dimensional scattering curve. Under these conditions, the normalized intensity scattered by a sample is

$$I_N(q) = \left[\frac{I_s(q)}{T_s\delta_s} - \frac{I_e(q)}{T_e\delta_e}\right] \quad (1)$$

where $I_N(q)$, δ, and T are the normalized measured intensity, the thickness, and the transmission of the sample (s) and the empty cell (e), respectively. To extract the coherent intensity scattered by the peptides, we subtracted the coherent intensity scattered by the solvent and the incoherent intensity scattered by the peptide and the solvent from the total scattered intensity. The coherent intensity scattered by the peptides in absolute units is then

$$I_A(q) = \frac{1}{K}[I_N(q) - (1 - C_p)I_D(q) - I_b] \quad (2)$$

where $I_D(q)$ is the normalized intensity scattered by the deuterated solvent, C_P is the peptide concentration in g cm^{-3}, I_b is the background scattering mainly due to the incoherent scattering of the hydrogenous peptides, and K is the contrast factor. The background scattering, I_b, was estimated using the Porod law, which gives the scattered intensity of a two-phase system at high q values:[39−41]

$$I(q) = \frac{K_p}{q^4} + I_b \quad (3)$$

where K_p is the Porod constant. I_b was estimated by fitting the last 10 data points (2.5−3.0 nm^{-1}) of the scattering curves, where the background scattering is dominant, using a Porod representation ($q^4I(q)$ vs q^4). Solutions and hydrogel samples for neutron experiments were prepared as described above using deuterated water directly in HELLMA quartz cells with an optical path length of 2 and 5 mm, depending on the sample concentration. Deuterated water (D_2O) was used instead of hydrogenated water to increase the contrast between the peptides and the solvent.

RESULTS AND DISCUSSION

In an earlier study we investigated the self-assembly of a series of octa-peptides that included FEF**E**F**K**FK and FEF**K**F**E**FK (F: phenylalanine; K: lysine; E: glutamic acid). These two peptides differ only by the position of the central E and K residues (Figure 1). In this earlier study, FTIR was used to show that both peptides had the same tendency to form β-sheet fibers. In addition, SANS experiments carried out at low concentration,

DOI: 10.1021/acs.biomac.6b01693
Biomacromolecules XXXX, XXX, XXX−XXX

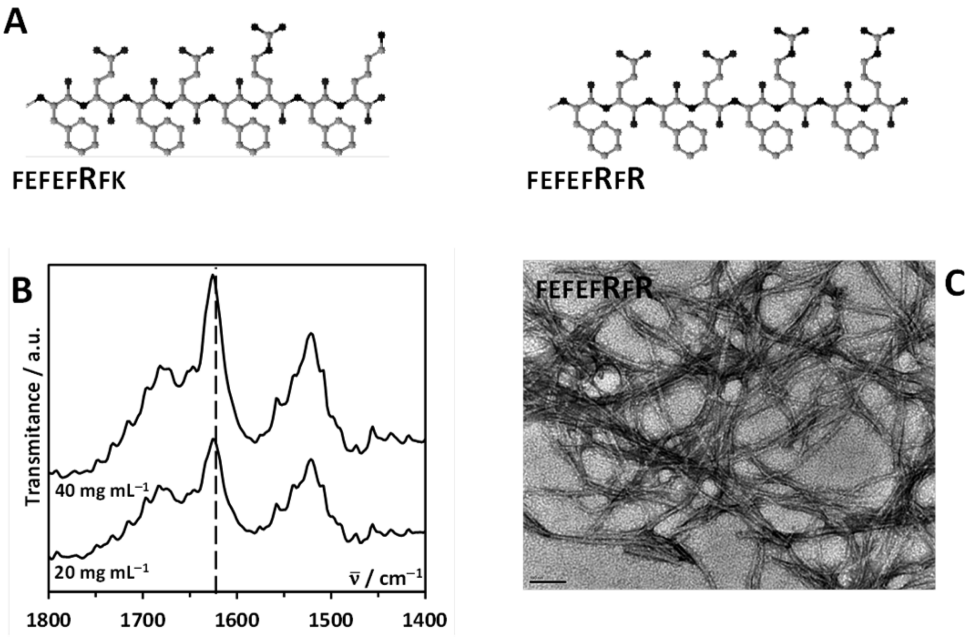

Figure 3. (A) Chemical structure of arginine (R) containing peptides. (B) FTIR spectra of FEFEF**R**F**R** sample at 5 mg mL^{-1} (β-sheet band: 1624 cm^{-1}). (C) TEM image obtained for FEFEF**R**F**R** sample (scale bar: 100 nm).

that is, below the critical gelation concentration (CGC), revealed that similar fibers were formed by both peptides.[17] One puzzling result obtained since that study has been the difference in mechanical properties of the hydrogels formed. Indeed, as can be seen from Figure 2A higher shear moduli, in particular, at higher peptide concentrations were obtained for FEF**K**F**E**FK. In addition, the temperature−concentration phase diagrams of these two systems were also found to differ significantly (Figure 2B). FEF**K**F**E**FK formed hydrogels at lower concentration (>5 mg mL^{-1}) that could not be melted, while FEF**E**F**K**FK formed hydrogels at higher concentration (>10 mg mL^{-1}) that could be melted into viscous liquids at high temperature. Based on our earlier work, our hypothesis was that the differences in mechanical properties and phase behavior were due to differences in network topologies rather than differences in fiber intrinsic properties. TEM supported this assumption. As can be seen from Figure 2C, TEM images show the formation of a network of uniform thin entangled fibers for FEF**E**F**K**FK with dimensions, 3−5 nm, which agrees with our earlier work. "Y" shaped branching points can be observed where one fiber "splits" into two fibers of the same dimensions. The branching of β-sheet forming peptides was discussed by Pochan and co-worker for a family of β-hairpin peptides. These authors suggested that branching was due to the mis-assembly of the peptides.[42] Keeping in mind that each fiber is formed by two β-sheets (Figure 1), it is reasonable to assume a similar origin for the "Y" shaped branching observed here. For FEF**K**F**E**FK, a slightly different network topology is observed. Although "Y" shaped branching of fibers can still be observed, thicker fiber bundles, formed from the association along their length of two or more fibers, can also be seen (Figure 2D). This suggests that the positions of K and E affects the tendency of the fibers to interact. It should be noted that at pH 3 these peptides and, therefore, the fibers they form carry a positive charge and that the presence of TFA in the sample will result in some level of charge screening that will promote peptide self-assembly and sample gelation. The position of the lysine residues affects the overall charge distribution on the fiber surface and therefore the way the electrostatic repulsion acts.[43,44] The different topologies observed for these two networks agree well with the observations above. Indeed, the association of fibers along their length is expected to result in stiffer fiber bundles and a stiffer network, resulting in a higher shear modulus. Fiber bundling is expected to increase with concentration, as fibers come into closer proximity; therefore, the effect on the mechanical properties is also expected, as observed, to be more marked at higher concentrations. In addition, this association tendency is thought to also promote the formation of a more stable percolated network resulting in a lower CGC and a reduced melting tendency. Indeed, fiber bundles are expected to be more difficult to melt/disassociate than "Y" branching points as the latter can be considered weak points.

It is well-known that hydrogel mechanical properties are very sensitive to network topology. A number of theoretical models can be found that describe the mechanical properties of hydrogels.[45] They usually relate the modulus of the hydrogel to the concentration through power laws. One such model was proposed by Jones and Marques for a network of semirigid fibers joined at frozen junction points.[46] It relates the shear modulus of the hydrogel to the sample concentration through

$$G' \sim C^{(3+FD)/(3-FD)} \quad (4)$$

where FD is the fractal dimension of interconnecting objects. For semirigid fibers, FD is expected to be in the range of 1.0−1.2 corresponding to an exponent of 2.0−2.3. The following power laws were obtained for our two peptides:

$$\text{FEF}\mathbf{E}\text{F}\mathbf{K}\text{FK} \Rightarrow G' \sim C^{2.4} \text{ and FEF}\mathbf{K}\text{F}\mathbf{E}\text{FK} \Rightarrow G' \sim C^{4.6}$$

A good agreement was obtained for the FEF**E**F**K**FK system with Jones and Marques model. The network topology observed for this system (uniform semirigid fibers connected at frozen junction points) resembles the most the network topology assumed in this model. For FEF**K**F**E**FK, a larger exponent than predicted was obtained. There are a number of reasons for the deviation from the model. First of all, the model

DOI: 10.1021/acs.biomac.6b01693
Biomacromolecules XXXX, XXX, XXX−XXX

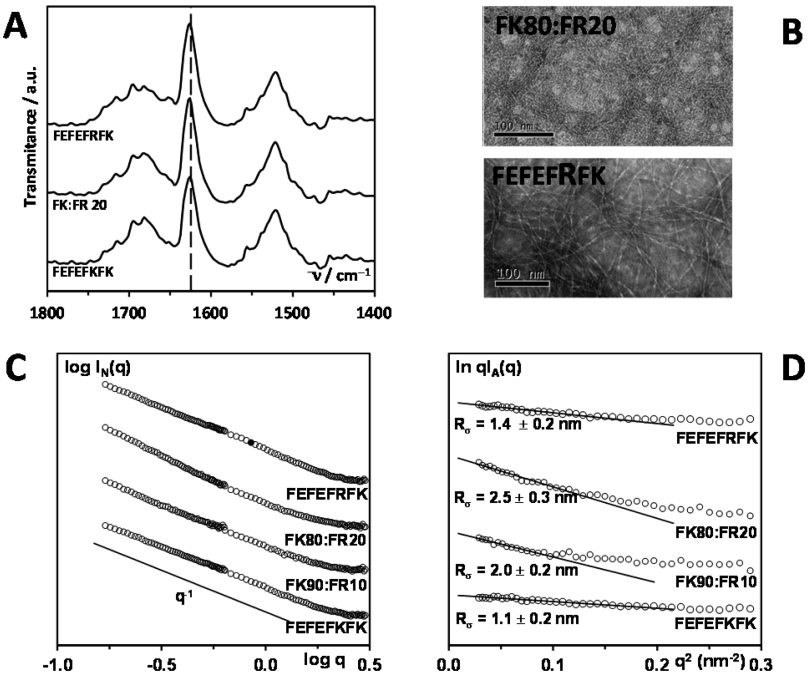

Figure 4. (A) FTIR spectra of hydrogels samples (β-sheet band: 1624 cm^{-1}); (B) TEM image obtained for hydrogel samples (scale bar: 100 nm); (C) SANS scattering pattern (log $I(q)$ vs log q) obtained for the sample below the CGC (5 mg mL^{-1}); (D) SANS scattering pattern at low q plotted in a $\ln[qI_A(q)]$ vs q^2 representation. Best fits of curves linear sections are presented with the corresponding values of R_σ extracted (see text for more details).

does not take into consideration fiber polydispersity (through bundle formation) and, therefore, variation in network basic element properties, such as stiffness. In addition, as the model was developed for polymeric systems, the concentration is assumed to directly relate to the concentration of connecting elements in the network. As shown by Ramzi et al., the presence in a polymeric network of pendant chains that do not participate in the network elasticity can result in a higher than expected exponent, as the "effective" network element concentration is lower than the polymer concentration.[47] In our case, there is no direct evidence of the presence of pendant chains. Nevertheless, the fiber thickening observed for FEF**K**FE**F**K system is thought to have a similar effect. Indeed, fiber bundles will act as a single element contributing to the network elasticity, resulting in a lower apparent network "effective" concentration and, therefore, in a higher exponent.

The results discussed above suggest that fiber association can be used to control network topology and, therefore, the mechanical properties of the peptide hydrogels. To confirm that such an approach can be used to design hydrogels with tailored properties, arginine residues were introduced in our peptide design by replacing one or both of the lysines. As mentioned in the introduction, arginine is expected to promote through its guanidine side group strong fiber−fiber interactions.

The following two sequences were designed: FEFEF**R**FK and FEFEF**R**F**R** (Figure 3A). For FEFEF**R**F**R**, opaque viscous solutions/precipitates were obtained at all concentrations. FTIR confirmed the adoption by this peptide of a β-sheet conformation (Figure 3B), and TEM revealed the presence of similar fibers as above (Figure 3C). The fibers though were observed to form, in this case, large bundles/aggregates, clearly showing that, as hypothesized, R promotes strong fiber−fiber interactions. To prevent the formation of such large scale aggregates and their precipitation, we decided to "dope" FEF**E**F**K**FK hydrogels with small amounts of FEFEF**R**F**R**, 10 and 20% (wt), keeping the overall sample peptide concentration constant. These two samples will be referred to as FK90:FR10 and FK80:FR20, respectively.

FK90:FR10 and FK80:FR20 were found to form slightly "hazy" hydrogels, while FEFEF**R**FK was found to form clear transparent hydrogels in the concentration range investigated. As can be seen from Figure 4A, FTIR results suggest that the introduction of arginine did not affect the peptides tendency to form β-sheets; indeed, similar relative peak intensities in the amide region were observed for all samples. The formation of fibrous networks was confirmed by TEM (Figure 4B).

A first series of SANS experiments was performed below the CGC of the samples in the dilute regime. In this regime, the scattering observed is dominated by the form factor of the diluted scattering entities. As can be seen from Figure 4C, all the samples scattering patterns present $a \sim q^{-1}$ behavior at low q typical of the scattering of fibers. For infinitely long rod-like structures, that is, semirigid fibers, in the q range investigated, the scattered intensity can be written as[39,48,49]

$$q^2 I_A(q) = \pi q C_p \mu_L f(qR_\sigma) + Cst \quad (5)$$

where μ_L is the mass per unit length of the rod in g mol^{-1} nm^{-1}, C_p is the peptide concentration in g cm^{-3}, and $f(qR_\sigma)$ represents the cross-section scattering, R_σ being the cross-section radius of gyration of the rod. Cst is a constant term taking into account interscattering effects. For $qR_\sigma < 1$, eq 5 reduces to[39,48−50]

$$qI_A(q) = \pi C_p \mu_L \exp\left(\frac{q^2 {R_\sigma}^2}{2}\right) \quad (6)$$

If the scattering observed is of the form described by eq 6, then at low q, a linear behavior should be obtained in a $\ln[qI_A(q)]$ versus q^2 representation. This is indeed the case as can be seen from Figure 4D. The cross-section radius of gyration, R_σ, of the

DOI: 10.1021/acs.biomac.6b01693
Biomacromolecules XXXX, XXX, XXX−XXX

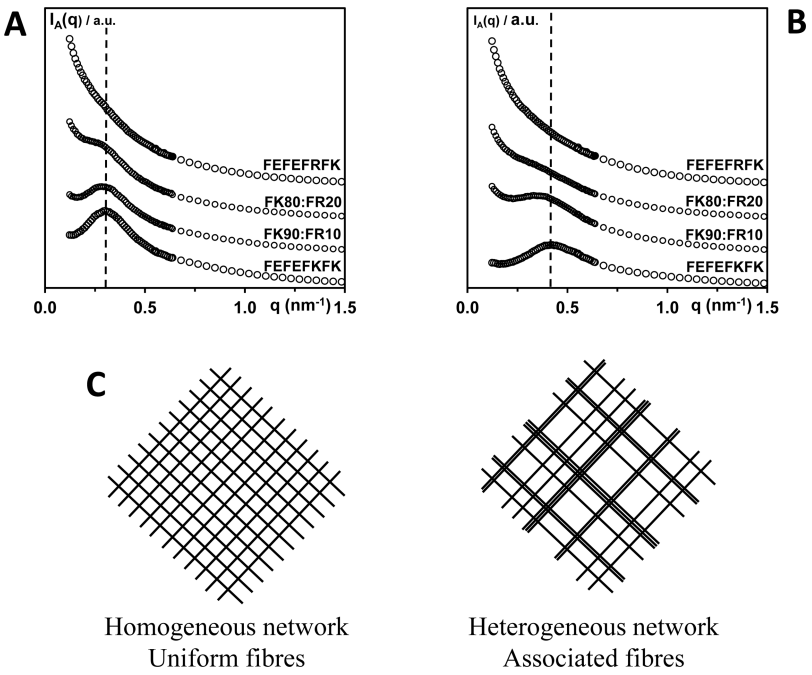

Figure 5. (A, B) SANS scattering pattern ($I_A(q)$ vs q) obtained for samples prepared at 20 mg mL^{-1} (A) and 30 mg mL^{-1} (B), above the CGC of the samples. (C) 2D idealized representation of the effect of fiber association/bundling on overall network topology.

fibers can be estimated from the slope of the linear section. If we assume that the fibers can be modeled by a plain infinitely long cylinder then R_σ is related to the diameter of the fiber, d, through $R_\sigma = \sqrt{d^2/8}$. As can be seen from Figure 4, for FEF**E**F**K**FK, a R_σ of 1.1 ± 0.2 nm was obtained corresponding to a fiber diameter of 3.1 ± 0.6 nm, in good agreement with our previous work and the TEM image in Figure 2. For FEFEF**R**FK, a slightly higher R_σ is obtained corresponding to a slightly larger fiber diameter of 4.0 ± 0.5 nm. For FK90:FR10 and FK80:FR20, larger R_σ are obtained corresponding to fiber diameters of 5.6 ± 0.6 and 7.1 ± 0.8 nm, respectively. From the FTIR and TEM results above, we can assume that the same basic β-sheet fibers are formed for all the systems, and therefore, the increase in fiber sizes below the CGC suggests the formation of fiber bundles through lateral fiber association. Indeed, it should be kept in mind that the scattering observed is the average scattering of all the rod-like objects, in this case, fibers and fiber bundles, present in the sample. Although the FEFEF**R**FK sample contains a larger nominal amount of arginine residues (12.5% of all residues are R in this sample compared to 5% for FK80:FR20 and 2.5% for FK90:FR10), this system shows a "lower" drive to fiber association/bundling. These results suggest that the localization of two R on the same peptide promotes strong fiber association and bundle formation.

In order to investigate the samples morphology, a second series of SANS experiments were carried out above the CGC, at 20 and 30 mg mL^{-1}. In this regime, the scattering observed is due to the overall sample morphology, that is, fibers and network. The results presented in Figure 5A,B confirm that the introduction of R affects the morphology of the sample.

For FEF**E**F**K**FK, a scattering peak is observed at 0.3 and 0.4 nm^{-1} for the 20 and 30 mg mL^{-1} samples, respectively. The presence of such a peak suggests that the samples' morphology is highly homogeneous and that a characteristic density fluctuation length is present across the sample. This density fluctuation length is related to the characteristic length scale of the morphology which in turn is related to the characteristic length scales of the two phases forming it: the low density phase (water rich phase, i.e., mesh size), and the high density phase (fiber rich phase: i.e., fiber cross-section).[50] As a result, if it is assumed that the fiber cross-section is significantly smaller than the network mesh size, the position of the scattering peak can be related through Bragg's law, $(2\pi)/q$ to the network mesh size ∼20 and 15 nm for the 20 and 30 mg mL^{-1} samples, respectively. As expected, the mesh size decreases with increasing peptide concentration as the density of fibers increases. It should be kept in mind that, as discussed above, for FEF**E**F**K**FK, no fiber association/aggregation is expected. In addition, at pH 3, this peptide and therefore the fibers carry a positive charge resulting in fiber−fiber repulsion. We hypothesize that as a result there is the formation of highly homogeneous fibers that "avoid" contact due to electrostatic repulsion, a highly homogeneous network and morphology is obtained with branching points and entanglements (no fiber association/bundling).

When FEFEF**R**F**R** is introduced (FK90:FR10 and FK80:FR20 samples), the peak scattering intensity decreases, while the scattering intensity at low q increases. These changes in scattering profiles suggest that the sample morphology becomes less homogeneous and that larger scattering entities form, respectively. As mentioned above, the scattering observed in this regime originates from the overall sample morphology, fibers and network; therefore, the increase of the scattering intensity at low q is thought to be related to the formation of fiber bundles as well as to the resulting increase in network mesh size (Figure 5C). It is interesting to note that the changes in scattering patterns are more pronounced at higher concentration. The drive of fiber association is indeed expected to increase with increasing concentration as the fibers are in closer proximity. These results seem to be supported by the TEM images (Figure 4B) showing a more coarse network topology for FK20:FR80 sample, although it should be kept in

DOI: 10.1021/acs.biomac.6b01693
Biomacromolecules XXXX, XXX, XXX−XXX

mind that TEM images can be misleading as the samples are subject to significant conditioning (see Materials and Methods) and the images give a 2D representation of a 3D network.

For the FEFEF**R**FK sample, a small shoulder can be observed at 20 mg mL^{-1}, while at 30 mg mL^{-1}, the scattering peak has disappeared altogether. For this sample, too, scattering at low q is observed to increase significantly again pointing toward the formation of larger scattering entities and a decrease in morphology homogeneity. The loss of morphological homogeneity, while fiber bundles form, is not surprising. Indeed, fiber lateral association as occurring here is not a controlled process, and therefore, fiber bundles of different sizes are expected to form. This is expected to lead to a polydispersed mesh size and diffuse scattering (Figure 5). Interestingly, the transparent appearance of the hydrogel formed with FEFEF**R**FK suggests that any morphological heterogeneity formed is below the half-micron size above where light scattering is observed. On the other hand, FK90:FR10 and FK80:FR20 form slightly hazy hydrogels, suggesting in this case morphological heterogeneities reach the half-micron scale. These observations suggest that the introduction of only one R on all the peptides leads to more "controlled" fiber association/aggregation, resulting in fiber bundles of limited size. On the other hand, introduction of FEFEFRFR leads to uncontrolled fiber association/aggregation, resulting in the formation of large bundles and, as discussed above, for pure FEFEF**R**F**R** sample to their precipitation.

As expected, the change in network topology has a strong effect on the mechanical properties of the hydrogels. In Figure 6, the dynamic storage shear moduli obtained for the 3 samples

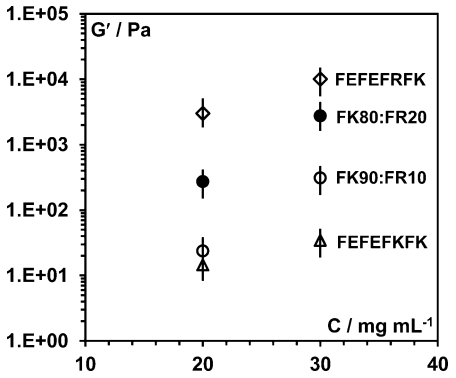

Figure 6. Dynamic shear storage moduli of hydrogels as a function of sample concentration.

at 20 and 30 mg mL^{-1} are presented. The introduction of FEFEF**R**F**R** results in a gradual increase in the G' of the sample. Surprisingly, FEFEF**R**FK forms stronger hydrogel at both concentrations, although as discussed above, the fiber association drive seems to be "weaker" for this sample. This clearly points out that in order to control the properties of the hydrogel the fiber association process needs to occur in a controlled fashion. Indeed, the bulk properties of the hydrogels will be a combination between the intrinsic properties of the fibers/fiber bundles and the overall properties of the network, which will depend on the mesh size and therefore on the level of fiber bundling. These results though clearly point out the importance of network topology in controlling the properties of this type of hydrogel.

CONCLUSIONS

We have investigated how network topology affects the mechanical properties of a family of β-sheet forming peptides whose design is based on the alternation of hydrophobic and hydrophilic residues. Our results clearly show that, in addition to the fiber intrinsic properties, the way these fibers self-assemble themselves to form a 3D percolated network has a significant impact on the final macroscopic properties of the resulting hydrogels. Taking advantage of the peptide design features used here, we have shown how, by design, in this specific case, introducing a highly interacting hydrophilic amino acid arginine, the fiber−fiber interaction can be manipulated to control the level of fiber lateral association/bundling. This approach allows carefully engineering by design not only the type of fiber formed, in our case, antiparallel β-sheet, but also the type of network topology formed, branched versus associated. The approach described in this work will be key for the design of hydrogels, exploiting β-sheet forming peptides with highly controlled mechanical properties, in particular, for the biomedical field.

ASSOCIATED CONTENT

Supporting Information

The Supporting Information is available free of charge on the ACS Publications website at DOI: 10.1021/acs.biomac.6b01693.

HPLC traces of the four peptides used in this work (PDF).

AUTHOR INFORMATION

Corresponding Author

*E-mail: a.saiani@manchester.ac.uk. Phone: +44 (0)161 306 5981.

ORCID

Alberto Saiani: 0000-0002-5504-8306

Present Address

§School of Science, Xi'an Jiaotong University, Xi'an, 710049, ShaanXi, P.R. China.

Notes

The authors declare no competing financial interest.

ACKNOWLEDGMENTS

The authors are grateful to the UK Engineering and Physical Sciences Research Council (EPSRC Fellowship Grant No. EP/K016210/1) and the University of Manchester KTA Programme for their financial support. J.G. is also grateful to the University Manchester Alumni fund and Peptisyntha (Solvay Group) for funding her scholarship. The authors are also grateful to the Forshungszentrum Jülich (FRJ-2) staff on diffractometer KWS-2 for their support. All research data supporting this publication are directly available within this publication.

REFERENCES

(1) Busseron, E.; Ruff, Y.; Moulin, E.; Giuseppone, N. Supramolecular self-assemblies as functional nanomaterials. *Nanoscale* **2013**, *5* (16), 7098−7140.

(2) Stephanopoulos, N.; Ortony, J. H.; Stupp, S. I. Self-assembly for the synthesis of functional biomaterials. *Acta Mater.* **2013**, *61* (3), 912−930.

DOI: 10.1021/acs.biomac.6b01693
Biomacromolecules XXXX, XXX, XXX−XXX

(3) Stupp, S. I.; Palmer, L. C. Supramolecular Chemistry and Self-Assembly in Organic Materials Design. *Chem. Mater.* **2014**, *26* (1), 507−518.
(4) Zhang, S. G. Fabrication of novel biomaterials through molecular self-assembly. *Nat. Biotechnol.* **2003**, *21* (10), 1171−1178.
(5) De Santis, E.; Ryadnov, M. G. Peptide self-assembly for nanomaterials: the old new kid on the block. *Chem. Soc. Rev.* **2015**, *44* (22), 8288−8300.
(6) Hamley, I. W. Peptide fibrillization. *Angew. Chem., Int. Ed.* **2007**, *46* (43), 8128−8147.
(7) Zhang, S. G. Emerging biological materials through molecular self-assembly. *Biotechnol. Adv.* **2002**, *20* (5−6), 321−339.
(8) Pugliese, R.; Gelain, F. Peptidic Biomaterials: From Self-Assembling to Regenerative Medicine. *Trends Biotechnol.* **2016**, DOI: 10.1016/j.tibtech.2016.09.004.
(9) Koutsopoulos, S. Self-assembling peptide nanofiber hydrogels in tissue engineering and regenerative medicine: Progress, design guidelines, and applications. *J. Biomed. Mater. Res., Part A* **2016**, *104* (4), 1002−1016.
(10) Worthington, P.; Pochan, D. J.; Langhans, S. A. Peptide Hydrogels - Versatile Matrices for 3D Cell Culture in Cancer Medicine. *Front. Oncol.* **2015**, *5* (92), n/a.
(11) Castillo Diaz, L. A.; Elsawy, M.; Saiani, A.; Gough, J. E.; Miller, A. F. Osteogenic differentiation of human mesenchymal stem cells promotes mineralization within a biodegradable peptide hydrogel. *J. Tissue Eng.* **2016**, *7*, n/a.
(12) Diana, M. L.; Eugen, B.; Geoffrey, J. P.; Aikaterini, L. Peptide Self-Assemblies for Drug Delivery. *Curr. Top. Med. Chem.* **2015**, *15* (22), 2277−2289.
(13) Zhiqiang, Y.; Quan, X.; Chenbo, D.; Su Seong, L.; Liqian, G.; Yiwen, L.; Mathew, D.; Ortenzio; Jun, W. Self-Assembling Peptide Nanofibrous Hydrogel as a Versatile Drug Delivery Platform. *Curr. Pharm. Des.* **2015**, *21* (29), 4342−4354.
(14) Zhang, S. G.; Holmes, T.; Lockshin, C.; Rich, A. Spontaneous Assembly of a Self-Complementary Oligopeptide to Form a Stable Macroscopic Membrane. *Proc. Natl. Acad. Sci. U. S. A.* **1993**, *90* (8), 3334−3338.
(15) Leon, E. J.; Verma, N.; Zhang, S. G.; Lauffenburger, D. A.; Kamm, R. D. Mechanical properties of a self-assembling oligopeptide matrix. *J. Biomater. Sci., Polym. Ed.* **1998**, *9* (3), 297−312.
(16) Zhang, S. G.; Altman, M. Peptide self-assembly in functional polymer science and engineering. *React. Funct. Polym.* **1999**, *41* (1−3), 91−102.
(17) Saiani, A.; Mohammed, A.; Frielinghaus, H.; Collins, R.; Hodson, N.; Kielty, C. M.; Sherratt, M. J.; Miller, A. F. Self-assembly and gelation properties of alpha-helix versus beta-sheet forming peptides. *Soft Matter* **2009**, *5* (1), 193−202.
(18) Maslovskis, A.; Guilbaud, J. B.; Grillo, I.; Hodson, N.; Miller, A. F.; Saiani, A. Self-Assembling Peptide/Thermoresponsive Polymer Composite Hydrogels: Effect of Peptideâ€"Polymer Interactions on Hydrogel Properties. *Langmuir* **2014**, *30* (34), 10471−10480.
(19) Elsawy, M. A.; Smith, A. M.; Hodson, N.; Squires, A.; Miller, A. F.; Saiani, A. Modification of β-Sheet Forming Peptide Hydrophobic Face: Effect on Self-Assembly and Gelation. *Langmuir* **2016**, *32* (19), 4917−4923.
(20) Bowerman, C. J.; Nilsson, B. L. Review self-assembly of amphipathic beta-sheet peptides: Insights and applications. *Biopolymers* **2012**, *98* (3), 169−184.
(21) Holmes, T. C.; de Lacalle, S.; Su, X.; Liu, G. S.; Rich, A.; Zhang, S. G. Extensive neurite outgrowth and active synapse formation on self-assembling peptide scaffolds. *Proc. Natl. Acad. Sci. U. S. A.* **2000**, *97* (12), 6728−6733.
(22) Sun, Y.; Li, W.; Wu, X.; Zhang, N.; Zhang, Y.; Ouyang, S.; Song, X.; Fang, X.; Seeram, R.; Xue, W.; He, L.; Wu, W. Functional Self-Assembling Peptide Nanofiber Hydrogels Designed for Nerve Degeneration. *ACS Appl. Mater. Interfaces* **2016**, *8* (3), 2348−2359.
(23) Mujeeb, A.; Miller, A. F.; Saiani, A.; Gough, J. E. Self-assembled octapeptide scaffolds for in vitro chondrocyte culture. *Acta Biomater.* **2013**, *9* (1), 4609−4617.
(24) Kisiday, J.; Jin, M.; Kurz, B.; Hung, H.; Semino, C.; Zhang, S.; Grodzinsky, A. J. Self-assembling peptide hydrogel fosters chondrocyte extracellular matrix production and cell division: Implications for cartilage tissue repair. *Proc. Natl. Acad. Sci. U. S. A.* **2002**, *99* (15), 9996−10001.
(25) Yan, C.; Mackay, M. E.; Czymmek, K.; Nagarkar, R. P.; Schneider, J. P.; Pochan, D. J. Injectable Solid Peptide Hydrogel as a Cell Carrier: Effects of Shear Flow on Hydrogels and Cell Payload. *Langmuir* **2012**, *28* (14), 6076−6087.
(26) Castillo Diaz, L. A.; Saiani, A.; Gough, J. E.; Miller, A. F. Human osteoblasts within soft peptide hydrogels promote mineralisation in vitro. *J. Tissue Eng.* **2014**, *5*, 2041731414539344.
(27) Bradshaw, M.; Ho, D. W.; Fear, M. W.; Gelain, F.; Wood, F. M.; Iyer, S. Designer self-assembling hydrogel scaffolds can impact skin cell proliferation and migration. *Sci. Rep.* **2014**, *4*, 6903.
(28) Roberts, D.; Rochas, C.; Saiani, A.; Miller, A. F. Effect of Peptide and Guest Charge on the Structural, Mechanical and Release Properties of beta-Sheet Forming Peptides. *Langmuir* **2012**, *28* (46), 16196−16206.
(29) Tang, C.; Miller, A. F.; Saiani, A. Peptide hydrogels as mucoadhesives for local drug delivery. *Int. J. Pharm.* **2014**, *465*, 427−435.
(30) Branco, M. C.; Pochan, D. J.; Wagner, N. J.; Schneider, J. P. Macromolecular diffusion and release from self-assembled beta-hairpin peptide hydrogels. *Biomaterials* **2009**, *30* (7), 1339−1347.
(31) Lindsey, S.; Piatt, J. H.; Worthington, P.; SÃ¶nmez, C.; Satheye, S.; Schneider, J. P.; Pochan, D. J.; Langhans, S. A. Beta Hairpin Peptide Hydrogels as an Injectable Solid Vehicle for Neurotrophic Growth Factor Delivery. *Biomacromolecules* **2015**, *16* (9), 2672−2683.
(32) Hwang, W. M.; Marini, D. M.; Kamm, R. D.; Zhang, S. Q. Supramolecular structure of helical ribbons self-assembled from a beta-sheet peptide. *J. Chem. Phys.* **2003**, *118* (1), 389−397.
(33) Davies, R. P. W.; Aggeli, A.; Beevers, A. J.; Boden, N.; Carrick, L. M.; Fishwick, C. W. G.; McLeish, T. C. B.; Nyrkova, I.; Semenov, A. N. Self-assembling beta-sheet tape forming peptides. *Supramol. Chem.* **2006**, *18* (5), 435−443.
(34) Lee, N. R.; Bowerman, C. J.; Nilsson, B. L. Sequence length determinants for self-assembly of amphipathic beta-sheet peptides. *Biopolymers* **2013**, *100* (6), 738−50.
(35) Lee, N. R.; Bowerman, C. J.; Nilsson, B. L. Effects of Varied Sequence Pattern on the Self-Assembly of Amphipathic Peptides. *Biomacromolecules* **2013**, *14* (9), 3267−3277.
(36) Gallivan, J. P.; Dougherty, D. A. Cation-pi interactions in structural biology. *Proc. Natl. Acad. Sci. U. S. A.* **1999**, *96* (17), 9459−9464.
(37) Schneider, C. P.; Shukla, D.; Trout, B. L. Arginine and the Hofmeister Series: The Role of Ion-Ion Interactions in Protein Aggregation Suppression. *J. Phys. Chem. B* **2011**, *115* (22), 7447−7458.
(38) Vondrek, J. Ã.; Mason, P. E.; Heyda, J.; Collins, K. D.; Jungwirth, P. The Molecular Origin of Like-Charge Arginine-Arginine Pairing in Water. *J. Phys. Chem. B* **2009**, *113* (27), 9041−9045.
(39) Higgins, J. S.; Benoit, H. C. *Polymer and Neutron Scattering*; Clarendon Press: Oxford, 1994.
(40) Roe, R.-J. *Methods of X-Ray and Neutron Scattering in Polymer Science*; Oxford University Press: New York, 2000.
(41) Guinier, A.; Fournet, G. *Small-Angle Scattering of X-rays*; John Wiley & Sons, Inc.: New York, 1955.
(42) Branco, M. C.; Nettesheim, F.; Pochan, D. J.; Schneider, J. P.; Wagner, N. J. Fast Dynamics of Semiflexible Chain Networks of Self-Assembled Peptides. *Biomacromolecules* **2009**, *10* (6), 1374−1380.
(43) Caplan, M. R.; Moore, P. N.; Zhang, S. G.; Kamm, R. D.; Lauffenburger, D. A. Self-assembly of a beta-sheet protein governed by relief of electrostatic repulsion relative to van der Waals attraction. *Biomacromolecules* **2000**, *1* (4), 627−631.
(44) Boothroyd, S.; Miller, A. F.; Saiani, A. From fibres to networks using self-assembling peptides. *Faraday Discuss.* **2013**, *166*, 195−207.

DOI: 10.1021/acs.biomac.6b01693
Biomacromolecules XXXX, XXX, XXX−XXX

(45) Guenet, J. M. Structure versus rheological properties in fibrillar thermoreversible gels from polymers and biopolymers. *J. Rheol.* **2000**, *44* (4), 947−960.
(46) Jones, J. L.; Marques, C. M. Rigid Polymer Network Models. *J. Phys.* **1990**, *51* (11), 1113−1127.
(47) Ramzi, M.; Rochas, C.; Guenet, J. M. Structure-properties relation for agarose thermoreversible gels in binary solvents. *Macromolecules* **1998**, *31* (18), 6106−6111.
(48) Guilbaud, J. B.; Saiani, A. Using small angle scattering (SAS) to structurally characterise peptide and protein self-assembled materials. *Chem. Soc. Rev.* **2011**, *40* (3), 1200−1210.
(49) Guenet, J.-M. *Thermoreversible Gelation of Polymers and Biopolymers*; Academic Press: London, 1992.
(50) Guilbaud, J.-B.; Saiani, A. Using small angle scattering (SAS) to structurally characterise peptide and protein self-assembled materials. *Chem. Soc. Rev.* **2011**, *40* (3), 1200−1210.

DOI: 10.1021/acs.biomac.6b01693
Biomacromolecules XXXX, XXX, XXX−XXX

Controlling self-assembling peptide hydrogel properties through network topology

Jie Gao[1,2,#], Claire Tang[1,2], Andrew M. Smith[1,2], Aline F. Miller[2,3] and Alberto Saiani[1,2]*

[1] School of Materials, The University of Manchester, Oxford road, Manchester, M13 9PL, UK

[2] Manchester Institute of Biotechnology, The University of Manchester, Oxford road, Manchester, M13 9PL, UK.

[3] School of Chemical Engineering and Analytical Sciences, The University of Manchester, Oxford road, Manchester, M13 9PL, UK

[#] Current address: School of Science, Xi'an Jiaotong University, Xi'an, 710049, ShaanXi, P.R. China

* Corresponding author. E-mail: a.saiani@manchester.ac.uk; Phone: +44 (0)161 306 5981

Electronic Supplementary Information:

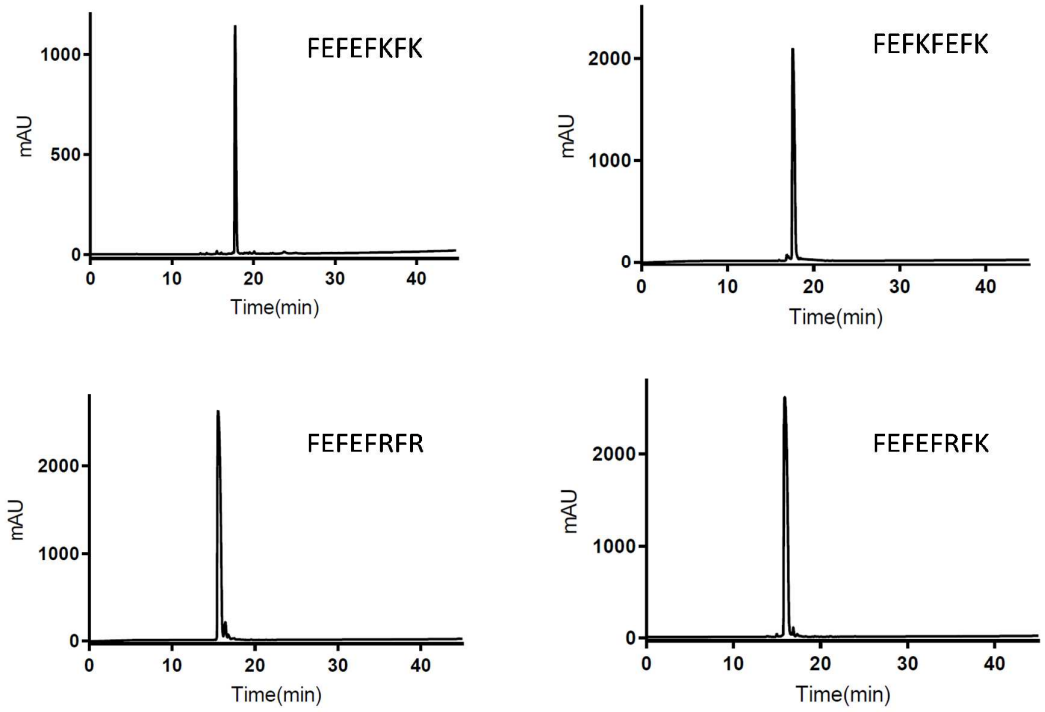

Figure ESI 1: HPLC traces of the four peptides used. (Method: The 1 mg ml^{-1} peptide solutions in 1% trifluoroacetic acid (TFA) in water/acetonitrile (50/50 V/V) were injected on the RP-HPLC column Phenomenex Jupiter 4µ Proteo column 90A° (250x4.66mm) equipped with UV detector (λ 220 nm). An elution gradient was used with a flow rate of 1ml/min that went from 90% solvent A (0.05% TFA in H_2O)/10% solvent B (0.05% TFA in CH_3CN) to 30% solvent A/70% solvent B in 45 minutes.)

Biomacromolecules
Msc: bm6b01693

The following graphic will be used for the TOC: